Gain-Scheduled Passivity-Based Tracking Control

Dylan Caverly

Supervised by Professor James Richard Forbes
Department of Mechanical Engineering
McGill University
Montreal, Canada

December 5, 2016

A thesis submitted to McGill University in partial fulfilment of the requirements of the Undergraduate Honours Program

Abstract

In this thesis, a controller synthesis method is presented for a gain-scheduled controller composed of a number of positive real controllers that contain internal models of reference command signals. Using the internal model principle as inspiration, and the Passivity Theorem to assure input-output stability, the proposed controller is designed to achieve excellent steady-state tracking of a reference command while maintaining input-output stability of the closed-loop system. The gain-scheduled nature of the internal models allows for a number of internal models to be simultaneously implemented. In particular, the first few terms of a Fourier series can be used as internal models to realize tracking of complicated reference commands. Two practical examples, one involving the tracking control of the modified tip velocity of a flexible-link manipulator, and the other involving the tracking control of the outlet temperature of a heat exchanger are presented.

Sommaire

Dans cette thèse, une méthode de synthèse de contrôleur est présentée pour un contrôleur de gain programmé, composé de plusiers contrôleurs réel positifs qui contiennent des modèles internes des signaux de commande de référence. S'inspirant du principe du modèle interne et du Théorème de la Passivité pour assurer la stabilité d'entrée-sortie, le contrôleur proposé est conçu pour obtenir un excellent suivi d'état d'équilibre d'une commande de référence tout en maintenant la stabilité entrée-sortie du système en boucle fermée. La nature de gain programmé des modèles internes permet plusieurs modeles internes d'être appliqué simultanément. En particulier, les premières termes d'une série Fourier peuvent être utilisés comme modèles internes pour réalizer le suivi de commandes de référence complexes. Deux exemples pratiques, l'un concernant le contrôle de suivi de la vitesse de pointe modifié d'un manipulateur de chaîne flexible, et l'autre visant le contrôle de suivi de la température de sortie d'une échangeur de chaleur sont présentés.

Acknowledgments

I am heartily thankful to my supervisor, Prof. James Richard Forbes, whose encouragement, guidance and support throughout the duration of this project enabled me to develop a greater understanding of this subject.

I would also like to extend my thanks to Ryan James Caverly and all of those that supported me throughout the course of this project for their instruction, help, advice and recommendations.

Dylan Caverly

Contents

List of Figures

List of Tables

Chapter 1

Introduction

1.1 Thesis Motivation, Objectives and Outline

The title of this thesis is *Gain-Scheduled Passivity-Based Tracking Control*. In this thesis we present a novel controller design method inspired by the Passivity Theorem and the internal model principle. These results are then used to control systems with passive input-output mappings. In particular, we control a flexible robotic manipulator and a heat exchanger.

1.1.1 Motivation and Objectives

Feedback control is able to realize many remarkable closed-loop properties such as disturbance rejection, noise mitigation, and command following. Moreover, these closed-loop traits can be realized even when the open-loop system dynamics are uncertain. Model uncertainty can never be reduced to zero and, as such, feedback control architectures that offer guarantees of closed-loop asymptotic stability (in, for example, an input-output or Lyapunov sense) are not only desired, but required if they are to have any real-world relevance.

The passive-systems framework is often employed to assure closed-loop input-output stability in the presence of model uncertainty. The strong form of the Passivity Theorem states that the negative feedback interconnection of a passive system and very strictly passive (VSP) system is input-output stable [1]. This result is robust to model uncertainty that does not violate the passive or VSP properties of the two systems in question. The Passivity Theorem has been employed in many engineering disciplines, including mechanical, aerospace, and electrical engineering.

Feedback control is often used to realize command following. One way to realize exact command following when the plant and controller are linear time-invariant (LTI) is through the internal model principle [2]. Neglecting disturbances, the internal model principle states that if either the LTI plant or the LTI controller has an internal model of the command, and the closed-loop system is asymptotically stable, then the error between the plant output and command asymptotically goes to zero as time goes to infinity. The internal model principle can also be used to reject disturbances when the disturbance's frequencies are known.

Although some controller synthesis methods currently exist that are inspired by either the internal model principle [3] or the Passivity Theorem [4], currently there are no controller synthesis methods that incorporate both ideas into one controller synthesis process to control systems with a passive input-output mapping.

This thesis brings together passive systems theory and the internal model principle. The first contribution of this thesis is a means to synthesize positive real (PR) controllers that contain an internal model of the designers choice. The second contribution of this thesis is using a previously presented passivity-based gain-scheduling architecture [5, 6] to gain schedule the PR controllers with internal models to, in effect, switch from one internal model to another, or use many internal models in a “Fourier series” to realize more command following. Moreover, by relying on passive systems theory, input-output stability results are robust to a large class of model uncertainty.

1.1.2 Outline

This thesis is structured as follows. Chapter 2 reviews the definition of a passive system, the Passivity Theorem, and other well-known results that are necessary for both the controller synthesis and numerical examples. Chapter 3 presents the proposed control architecture, inspired by the Passivity Theorem and Internal Model Principle. In Chapter 4, the proposed controller is tested in two numerical examples. First, a single controller is used to control the μ-tip velocity of a flexible-link manipulator, then a set of gain-scheduled controllers are implemented to control the output temperature of a single tube-in-shell heat exchanger. Finally, concluding remarks and suggestions for future work are presented in Chapter 5.

Chapter 2

Preliminaries

2.1 Notation

$\mathbf{A}$	an $n \times m$ matrix,
$\mathbf{1}$	an identity matrix of appropriate dimension,
$\mathcal{G} : L_{2e} \to L_{2e}$	an operator that maps L_{2e} signals to L_{2e} signals,
$\mathbf{A} = \mathbf{A}^{\mathsf{T}} > 0$	a symmetric positive definite matrix,
$\mathbf{A} = \mathbf{A}^{\mathsf{T}} \geq 0$	a symmetric positive semidefinite matrix,
$\mathbf{A} = \mathbf{A}^{\mathsf{T}} < 0$	a symmetric negative definite matrix,
$\mathbf{A} = \mathbf{A}^{\mathsf{T}} \leq 0$	a symmetric negative semidefinite matrix,

In the first numerical example provided in Chapter 4, we will use Vectrix notation, as described in [7, 8]. Briefly,

$\underset{\rightarrow}{v}$	a physical vector, independent of reference frame,
$\mathcal{F}_a$	reference frame defined by orthonormal basis vectors $\underset{\rightarrow}{a}_1$, $\underset{\rightarrow}{a}_2$, and $\underset{\rightarrow}{a}_3$,
$\underset{\rightarrow}{\mathcal{F}}_a = \begin{bmatrix} \underset{\rightarrow}{a}_1 & \underset{\rightarrow}{a}_2 & \underset{\rightarrow}{a}_3 \end{bmatrix}^\mathsf{T}$	a vectrix of orthonormal basis vectors forming a reference frame,
$\mathbf{v}_a^\mathsf{T} = \begin{bmatrix} v_a^1 & v_a^2 & v_a^3 \end{bmatrix}$	a column matrix representing the physical vector $\underset{\rightarrow}{v}$ expressed in $\mathcal{F}_a$,
$\underset{\rightarrow}{v}^{\cdot a}$	time derivative of $\underset{\rightarrow}{v}$ with respect to $\mathcal{F}_a$.

2.2 Passive Systems Theory

In this section passive systems theory is briefly reviewed. See [1] or [9] for details. To begin, a function $\mathbf{u} \in L_2$ if

$$\|\mathbf{u}\|_2 = \sqrt{\int_0^\infty \mathbf{u}^\mathsf{T}(t)\mathbf{u}(t)dt} < \infty, \tag{2.1}$$

and $\mathbf{u} \in L_{2e}$ if

$$\|\mathbf{u}\|_{2T} = \sqrt{\int_0^T \mathbf{u}^\mathsf{T}(t)\mathbf{u}(t)dt} < \infty, \quad \forall T \in \mathbb{R}^+. \tag{2.2}$$

A function $\mathbf{u} \in L_\infty$ if

$$\|\mathbf{u}\|_\infty = \sup_{t \in \mathbb{R}^+} \left[\max_{i=1\cdots n} |u_i(t)| \right] < \infty. \tag{2.3}$$

A general square system with inputs $\mathbf{u} \in L_{2e}$ and outputs $\mathbf{y} \in L_{2e}$ mapped through the operator $\boldsymbol{\mathcal{G}} : L_{2e} \rightarrow L_{2e}$ is very strictly passive (VSP) if there exists a constants $0 < \delta < \infty$, $0 < \epsilon < \infty$, and β such that [9]

$$\int_0^T \mathbf{y}^\mathsf{T}(t)\mathbf{u}(t)\mathrm{d}t \geq \delta \int_0^T \mathbf{u}^\mathsf{T}(t)\mathbf{u}(t)\mathrm{d}t + \epsilon \int_0^T \mathbf{y}^\mathsf{T}(t)\mathbf{y}(t)\mathrm{d}t + \beta, \quad \forall \mathbf{u} \in L_{2e}, \ \forall T \in \mathbb{R}^+. \tag{2.4}$$

When $\epsilon = \delta = 0$ the system is passive, when $\delta = 0$ the system is output strictly passive (OSP), and when $\epsilon = 0$ the system is input strictly passive (ISP). The scalar β is related to the initial conditions of the system.

Consider the negative feedback interconnection of $\boldsymbol{\mathcal{G}}_1 : L_{2e} \to L_{2e}$ and $\boldsymbol{\mathcal{G}}_2 : L_{2e} \to L_{2e}$, as shown in Fig. 2.1. The weak version of the Passivity Theorem states that the negative feedback interconnection of a passive system and an ISP system is input-output stable [9], while the strong form of the Passivity Theorem states that the negative feedback interconnection of a passive system and a VSP system is input-output stable [1]. In terms of Fig. 2.1, it matters not which of the systems, $\boldsymbol{\mathcal{G}}_1 : L_{2e} \to L_{2e}$ or $\boldsymbol{\mathcal{G}}_2 : L_{2e} \to L_{2e}$, is the passive one.

A passive system will have a PR transfer matrix function or a PR state-space realization that is minimal. An OSP system will have a strictly positive real (SPR) transfer matrix function or a SPR state-space realization that is minimal. A VSP system will have a SPR transfer matrix function or SPR state-space realization that is minimal with a feedthrough term. The definition of PR and SPR (for the case of no feedthrough) are as follows.

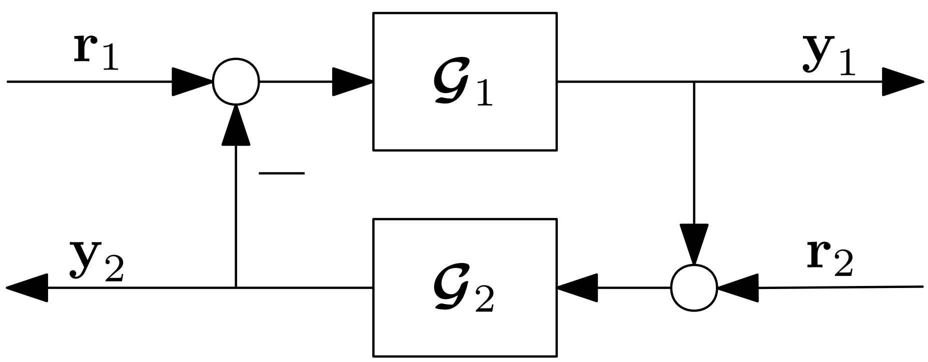

Fig. 2.1: Negative feedback interconnection of two systems.

Lemma 2.2.1. *(Kalman-Yakubovic-Popov (KYP) Lemma [1, 10]). Consider the LTI system*

$$\dot{\mathbf{x}} = \mathbf{A}\mathbf{x} + \mathbf{B}\mathbf{u}, \quad \mathbf{x}(0) = \mathbf{x}_0,$$
$$\mathbf{y} = \mathbf{C}\mathbf{x},$$

where $\mathbf{x} \in \mathbb{R}^n, \mathbf{u}, \mathbf{y} \in \mathbb{R}^m$*,* $\mathbf{A} \in \mathbb{R}^{n\times n}, \mathbf{B} \in \mathbb{R}^{n\times m}$*, and* $\mathbf{C} \in \mathbb{R}^{m\times n}$*, and* $(\mathbf{A}, \mathbf{B}, \mathbf{C})$ *is a minimal state-space realization. The system is PR if and only if there exist* $\mathbf{P} \in \mathbb{R}^{n\times n}$ *and* $\mathbf{Q} \in \mathbb{R}^{n\times n}$ *where* $\mathbf{P} = \mathbf{P}^\mathsf{T} > 0$ *and* $\mathbf{Q} = \mathbf{Q}^\mathsf{T} \geq 0$ *such that*

$$\mathbf{P}\mathbf{A} + \mathbf{A}^\mathsf{T}\mathbf{P} = -\mathbf{Q}, \tag{2.5}$$
$$\mathbf{P}\mathbf{B} = \mathbf{C}^\mathsf{T}.$$

If $\mathbf{Q} = \mathbf{Q}^\mathsf{T} > 0$ *satisfies the Lyapunov equation* (2.5)*, the system is SPR.*

When considering the negative feedback interconnection of the PR system and the SPR system without a feedthrough matrix, using Lyapunov stability theory, it can be shown that the origin of the closed-loop system is globally asymptotically stable. See [11] for details.

2.3 Internal Model Principle

Consider the negative feedback interconnection shown in Fig. 2.2 once more, and assume that both $\boldsymbol{\mathcal{G}}_1$ and $\boldsymbol{\mathcal{G}}_2$ are single-input single-output (SISO) systems with transfer function representations $g_1(s)$ and $g_2(s)$, respectively. Additionally, assume that the closed-loop system is asymptotically stable. The internal model principal states that if either $g_1(s)$ and $g_2(s)$ has an internal model of the reference command $r(s)$, then the output $y(s)$ will track the reference command with zero steady-state tracking error as $t \to \infty$ when there are no disturbances [2].

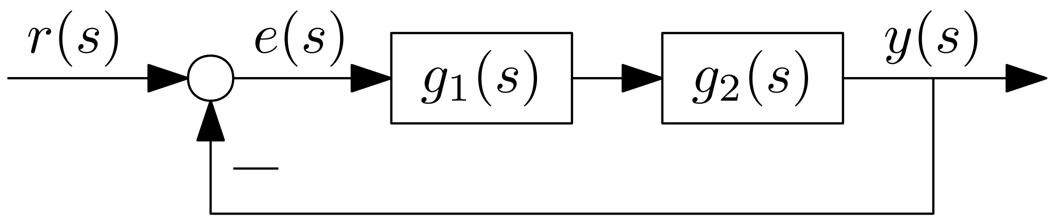

Fig. 2.2: Negative feedback interconnection of two systems.

2.4 Passivity-Based Gain-Scheduled Control

Consider the negative feedback interconnection of a gain-scheduled controller and plant shown in Fig. 2.3. This gain-scheduled control architecture is a SISO specialization of the architecture presented in [5, 6]. The scheduling signals, which may be a function of time or some other variable such as the plant output, are assumed to satisfy $s_i(t) \in L_2 \cap L_\infty$ and $\sum_{i=1}^{N} s_i^2(t) \geq \alpha > 0$, but are otherwise arbitrary. As discussed in [12], a straightforward modification of the proof presented in [5, 6] shows that if each $h_i(s)$ $i = 1, 2, \ldots, N$ is PR (i.e., the input-output mappings of each $y_i(s) = h_i(s)u_i(s)$ are passive), then the input-output map of the overall gain-scheduled controller is passive. From the Passivity Theorem, provided the plant is VSP, then the negative feedback interconnection of the VSP plant and passive gain-scheduled controller is input-output stable.

2.5 Fourier Convergence Theorem

Theorem 2.5.1. *Let $f(x)$ be a piecewise regular function on $x \in [-L, L]$ with a finite number of discontinuities and a finite number of discontinuities, maxima and minima over the interval, and*

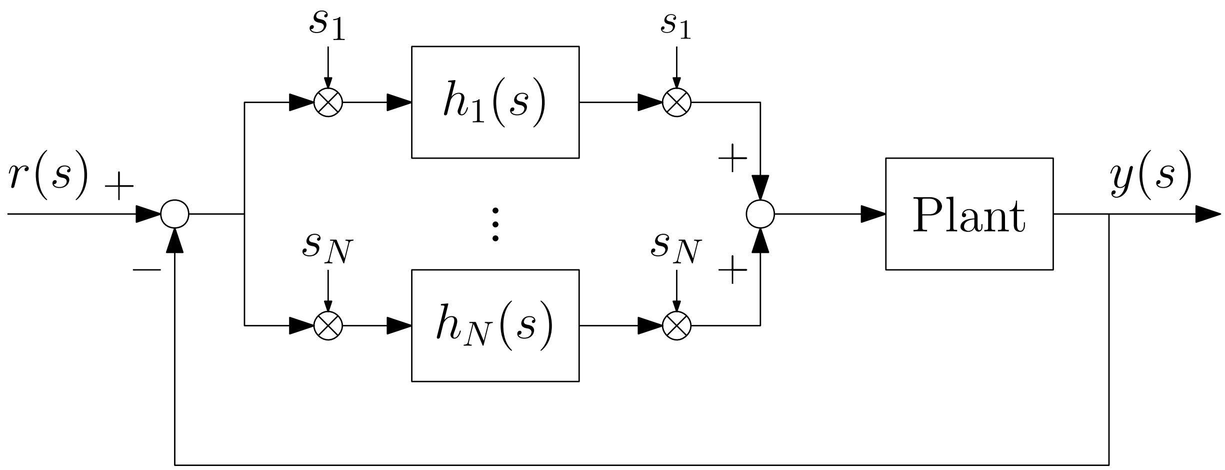

Fig. 2.3: Gain-scheduled controller and plant in a negative feedback interconnection.

let f be periodic with period $2L$, then f can be described by a Fourier series

$$f(x) = \frac{a_0}{2} + \sum_{n=1}^{\infty} a_n \cos\left(\frac{n\pi x}{L}\right) + b_n \sin\left(\frac{n\pi x}{L}\right),$$

where $n \in \mathbb{N}$. The constant Fourier coefficients a_0, a_n and b_n can be calculated from $f(x)$ [13].

2.6 The Rayleigh-Ritz Method

The Rayleigh-Ritz method can be used to convert the partial differential differential equations associated with the elastic mechanics of a system to a reasonable system of ordinary differential equations. The elastic deformation of a system, u_e, is expressed as a sum of a set of independent basis function. Written explicitly, this is given by

$$u_e(x,t) = \sum_{i=1}^{N} \Psi_i(x) q_{e_i}(t),$$

where N is the number of basis functions, $\Psi_i(x)$ spatially-dependent basis functions and q_{e_i} are time-dependent elastic coordinates. The basis functions must be carefully selected to satisfy all appropriate forced boundary conditions, and be differentiable to the same degree as the strain energy.

Chapter 3

Controller Synthesis Method

The controller synthesis method presented in this thesis is inspired by the Passivity Theorem and the internal model principle. The proposed controller synthesis method is introduced in two parts. First, the design of a PR controller with an internal model is presented, followed by the design of a gain-scheduled controller composed of multiple PR controllers with internal models.

3.1 PR Controller Synthesis with Internal Model

Consider an LTI plant $\boldsymbol{\mathcal{G}}_p : L_{2e} \to L_{2e}$ expressed in terms of a minimal state-space as

$$\begin{aligned}\dot{\mathbf{x}}_p &= \mathbf{A}_p\mathbf{x}_p + \mathbf{B}_p u, \quad \mathbf{x}_p(0) = \mathbf{x}_{p,0},\\ y &= \mathbf{C}_p\mathbf{x}_p,\end{aligned}$$

where $\mathbf{x}_p \in \mathbb{R}^n$ is the system state, $u \in \mathbb{R}$ is the control input, and $y \in \mathbb{R}$ is the system output. The constant state-space matrices are defined as $\mathbf{A}_p \in \mathbb{R}^{n\times n}$, $\mathbf{B}_p \in \mathbb{R}^{n\times m}$, and $\mathbf{C}_p \in \mathbb{R}^{m\times n}$, where

$m = 1$.

The internal model of the reference signal is written in state-space form as

$$\dot{\mathbf{x}}_i = \mathbf{A}_i \mathbf{x}_i + \mathbf{B}_i u_i, \quad \mathbf{x}_i(0) = \mathbf{x}_{i,0},$$
$$y_i = \mathbf{C}_i \mathbf{x}_i,$$

where $\mathbf{x}_i \in \mathbb{R}^{n_i}$ is the internal model state, $u_i \in \mathbb{R}$ is the internal model input, and $y_i \in \mathbb{R}$ is the internal model output. The state-space matrices of the internal model are defined as $\mathbf{A}_i \in \mathbb{R}^{n_i \times n_i}$, $\mathbf{B}_i \in \mathbb{R}^{n_i \times m_i}$, and $\mathbf{C}_i \in \mathbb{R}^{m_i \times n_i}$, where $m_i = 1$, and together form a minimal state-space realization.

The synthesis of the PR controller with internal model is described in the following steps.

1. Design a linear quadratic Gaussian (LQG) controller for the plant $\boldsymbol{\mathcal{G}}_p$. This controller has state-space realization $(\mathbf{A}_{_{LQG}}, \mathbf{B}_{_{LQG}}, \mathbf{C}_{_{LQG}}, \mathbf{D}_{_{LQG}})$, where

$$\mathbf{A}_{_{LQG}} = \mathbf{A}_p - \mathbf{B}_p \mathbf{K}_{_{LQG}} - \mathbf{L}_{_{LQG}} \mathbf{C}_p,$$
$$\mathbf{B}_{_{LQG}} = \mathbf{L}_{_{LQG}} = \mathbf{P}_2 \mathbf{C}_p^\mathsf{T} \mathbf{W}^{-1},$$
$$\mathbf{C}_{_{LQG}} = \mathbf{K}_{_{LQG}} = \mathbf{R}^{-1} \mathbf{B}_p^\mathsf{T} \mathbf{P}_1,$$
$$\mathbf{D}_{_{LQG}} = \mathbf{0},$$

$\mathbf{R} = \mathbf{R}^\mathsf{T} > 0$, and $\mathbf{W} = \mathbf{W}^\mathsf{T} > 0$. The matrices $\mathbf{P}_1 = \mathbf{P}_1^\mathsf{T} > 0$ and $\mathbf{P}_2 = \mathbf{P}_2^\mathsf{T} > 0$ are solutions to the algebraic Riccati equations

$$\mathbf{A}_p^\top \mathbf{P}_1 + \mathbf{P}_1 \mathbf{A}_p - \mathbf{P}_1 \mathbf{B}_p \mathbf{R}^{-1} \mathbf{B}_p^\top \mathbf{P}_1 + \mathbf{Q} = \mathbf{0},$$
$$\mathbf{A}_p \mathbf{P}_2 + \mathbf{P}_2 \mathbf{A}_p^\top - \mathbf{P}_2 \mathbf{C}_p^\top \mathbf{W}^{-1} \mathbf{C}_p \mathbf{P}_2 + \mathbf{V} = \mathbf{0},$$

where $\mathbf{Q} = \mathbf{Q}^\top \geq 0$ and $\mathbf{V} = \mathbf{V}^\top \geq 0$. See Fig. 3.1 for a block diagram representation of Step 1.

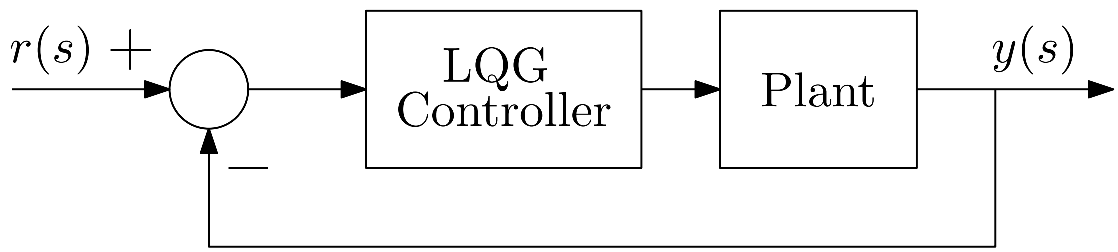

Fig. 3.1: Step 1 of the PR controller synthesis method with internal model in Section 3.1.

2. Cascade the LQG controller with the internal model, giving a controller of the form

$$\mathbf{A}_c = \begin{bmatrix} \mathbf{A}_{LQG} & \mathbf{0} \\ \mathbf{B}_i \mathbf{C}_{LQG} & \mathbf{A}_i \end{bmatrix}, \quad \mathbf{B}_c = \begin{bmatrix} \mathbf{B}_{LQG} \\ \mathbf{0} \end{bmatrix},$$
$$\mathbf{C}_c = \begin{bmatrix} \mathbf{0} & \mathbf{C}_i \end{bmatrix}, \qquad \mathbf{D}_c = \mathbf{0}.$$

See Fig. 3.2 for a block diagram representation of Step 1.

3. Solve for $\mathbf{P} = \mathbf{P}^\top > 0$ that minimizes the objective function

$$\mathcal{J}(\mathbf{P}) = \operatorname{tr}\left(\left(\mathbf{C}_c - \mathbf{B}^\top \mathbf{P}\right)^\top \left(\mathbf{C}_c - \mathbf{B}^\top \mathbf{P}\right) \right),$$

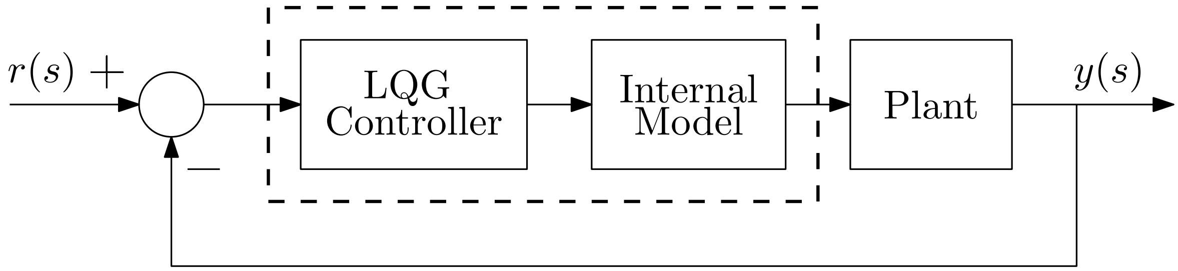

Fig. 3.2: Step 2 of the PR controller synthesis method with internal model in Section 3.1.

while satisfying the Lyapunov equation

$$\mathbf{P}\mathbf{A}_c + \mathbf{A}_c^{\mathsf{T}}\mathbf{P} \leq 0.$$

4. The solution **P** is used to solve for the new controller output matrix $\mathbf{C}_{c_2}$, given by

$$\mathbf{C}_{c_2} = \mathbf{B}^{\mathsf{T}}\mathbf{P}.$$

The new controller, with state-space realization $(\mathbf{A}_c, \mathbf{B}_c, \mathbf{C}_{c_2}, \mathbf{D}_c)$ now contains an internal model of the reference signal and is PR. Note that although not necessary in ensuring positive realness, the objective function $\mathcal{J}(\mathbf{P})$ is chosen in Step 3 so that $\mathbf{C}_{c_2}$ is as close to $\mathbf{C}_c$ as possible, while ensuring the new controller is PR.

3.2 Gain-Scheduled Controller Synthesis

The controller synthesis method of Section 3.1 is used to design N PR controllers, each with an internal model of a reference signal. The N controllers are gain-scheduled using the architecture presented in [5, 6] and shown in Fig. 2.3, which yields an overall gain-scheduled controller that is passive. The overall controller output is a weighted sum of the outputs of each individual controller, given by

$$y_c(t) = \sum_{j=1}^{N} s_j(t) y_j(t),$$

where $y_j(t)$ is the output of the j^{th} PR controller, and the scheduling signals $s_j(t)$, $j = 1, \ldots, N$ satisfy $s_j(t) \in L_2 \cap L_\infty$ and $\sum_{j=1}^{N} s_j^2(t) \geq \alpha > 0$. Following the gain-scheduling architecture of [5, 6], the input to each individual controller is also scheduled as $u_j(t) = s_j(t)e(t) = s_j(t)(r(t) - y(t))$, where u_j is the input to the j^{th} PR controller, and $e(t) = r(t) - y(t)$ is the tracking error.

3.3 Analysis and Discussion

The gain-scheduled controller obtained following the synthesis method presented in Sections 3.1 and 3.2 is passive. Assuming that the plant is VSP, the strong form of the Passivity Theorem guarantees that the closed-loop system is input-output stable, and $e(t) \in L_2$ if $r \in L_2$. It should be noted that this result also holds if the plant is uncertain or nonlinear, as long as it is VSP. In practice, it is quite possible that the plant will be OSP, but it is unlikely that it will be VSP, meaning the Passivity Theorem would technically not be satisfied.

Although the internal model principle is used as inspiration in this thesis, it cannot be directly shown that $e \to 0$ as $t \to \infty$ as the traditional internal model principle does. However, if it can be shown that $e(t) \in L_2$ and $\dot{e}(t) \in L_2$, then $e(t) \to 0$ as $t \to \infty$; this will be the subject of future work.

In general, the reference command signal may not be in L_2. For instance, $r(t) = \sin(\omega t)$ is not in L_2. In the case of a periodic signal that is not in L_2, a work-around to the issue of it not being in L_2 is to multiply the periodic signal by a slowly decaying exponential. For example, if the reference command $r(t) = \sin(\omega t)$ is to be tracked, the modified command $r(t) = e^{-\lambda t}\sin(\omega t)$ can be used, where $0 < \lambda < \infty$ is extremely small, with a time constant that is possibly on the order of years or decades. The resulting signal will be in L_2, which leads to a guarantee that the tracking error will be in L_2. Note, such a modification would not be needed in practice, but is technically needed to assure input-output stability via the Passivity Theorem.

An alternative to gain-scheduling many controllers that each include internal models is to design a single controller that contains one large internal model. In this method, a single internal model that includes the first few Fourier series modes of the reference command signal could be chosen. The controller synthesis proposed in this thesis is more flexible than this method, since the influence of each internal model can be adjusted to track a large range of signals. The scheduling signals can even be dynamically adjusted to track a time-varying reference command signal.

Chapter 4

Numerical Examples

4.1 Flexible-Link Manipulator

Consider a flexible-link manipulator with a tip mass, with parameters from Table 4.1 shown in Fig. 4.1. In this system, a torque is applied at the hub, in order to control the tip position and velocity. Using the proposed controller synthesis method in Section 3, a single passive controller is designed to track a given reference command signal.

Table 4.1: Numerical parameters describing the reference signal used in the numerical example.

Parameters	**Variable**	**Value**	**Units**
Tip Mass	m_{tip}	100	kg
Beam Length	l	1	m
Beam Linear Density	σ	0.2332	$\frac{\text{kg}}{\text{m}}$
Beam Flexible Rigidity	EI	5.41	N m^2
Hub Radius	r	0.3	m
Hub Second Moment of Inertia	I_{hub}	6.6×10^{-3}	kg m^2

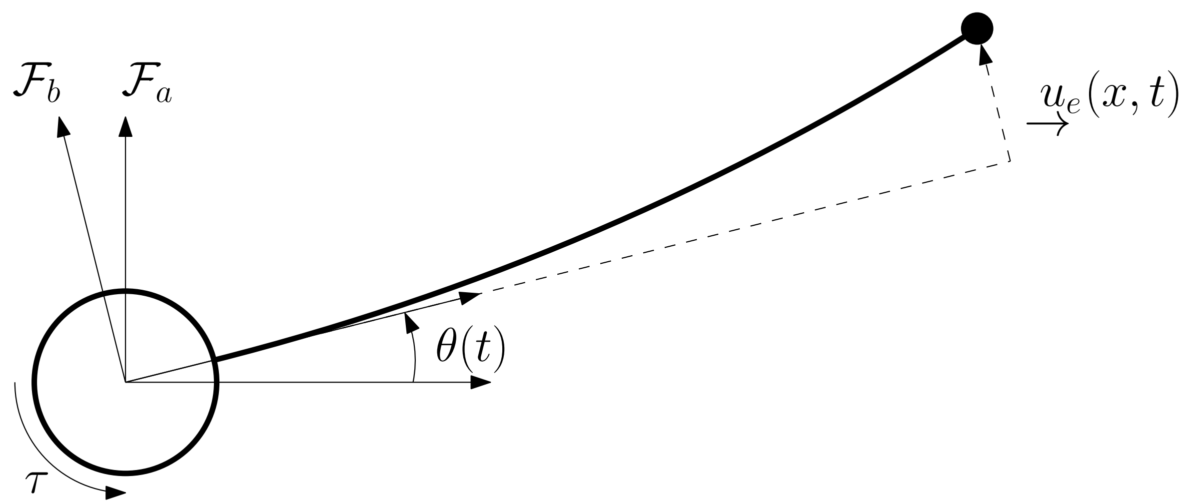

Fig. 4.1: Flexible-link manipulator with tip mass.

4.1.1 Dynamic Modelling

An inertial reference frame $\mathcal{F}_a$, defined by orthonormal basis vectors $\underset{\rightarrow}{a}_1$, $\underset{\rightarrow}{a}_2$, and $\underset{\rightarrow}{a}_3$, is chosen as a datum. The reference frame $\mathcal{F}_b$, defined by orthonormal basis vectors $\underset{\rightarrow}{b}_1$, $\underset{\rightarrow}{b}_2$, and $\underset{\rightarrow}{b}_3$, rotates with the rigid hub of the manipulator. The angle of rotation between $\mathcal{F}_b$ and $\mathcal{F}_a$ is θ. The spatial coordinate x is used to describe the position along $\underset{\rightarrow}{b}_1$ relative to the centre of the hub. In this example, the elastic deformation $\mathbf{u}_e^{\mathsf{T}} = \begin{bmatrix} 0 & u_e(x,t) & 0 \end{bmatrix}$ of the link is the representation of u_e in $\mathcal{F}_b$. This deflection is approximated using the Rayleigh-Ritz method. In this case, the geometric boundary conditions are

$$u_e(0,t) = 0, \quad \left.\frac{\partial u_e}{\partial x}\right|_{x=0} = 0, \quad \left.\frac{\partial}{\partial x}\left(EI\,\frac{\partial^2 u_e}{\partial x^2}\right)\right|_{x=L} = 0 \quad \text{and} \quad \left.EI\,\frac{\partial^2 u_e}{\partial x^2}\right|_{x=L} = 0.$$

One set of basis functions which satisfy these geometric boundary conditions are

$$\psi_i(x) = x^{i+1}, \quad i = 1, \ldots N.$$

For this numerical example, the first three basis functions are used to approximate the link's deflection. These basis functions satisfy the first two boundary conditions. Therefore, in vectrix notation, the elastic deflection of any point in the beam is

$$\underset{\rightarrow}{u}_e = \underset{\rightarrow}{\boldsymbol{\mathcal{F}}}_a^{\mathsf{T}} \mathbf{u}_e = \underset{\rightarrow}{\boldsymbol{\mathcal{F}}}_a^{\mathsf{T}} \begin{bmatrix} 0 & 0 & 0 \\ x^2 & x^3 & x^4 \\ 0 & 0 & 0 \end{bmatrix} \begin{bmatrix} q_{e_1}(t) \\ q_{e_2}(t) \\ q_{e_3}(t) \end{bmatrix} = \underset{\rightarrow}{\boldsymbol{\mathcal{F}}}_a^{\mathsf{T}} \boldsymbol{\Psi}(x) \mathbf{q}_e(t).$$

When the beam is rigid, the position of any point along the beam can be described by

$$\underset{\rightarrow}{\rho}(x) = \underset{\rightarrow}{\boldsymbol{\mathcal{F}}}_b^{\mathsf{T}} \begin{bmatrix} x + r \\ 0 \\ 0 \end{bmatrix},$$

and $\boldsymbol{\rho}_b$ represents the physical vector $\underset{\rightarrow}{\rho}$ in $\boldsymbol{\mathcal{F}}_b$. The kinetic and potential energies of the system can be described by

$$\begin{aligned} T &= \tfrac{1}{2}\dot{\mathbf{q}}^{\mathsf{T}}\mathbf{M}\dot{\mathbf{q}}, \\ V &= \tfrac{1}{2}\mathbf{q}^{\mathsf{T}}\mathbf{K}\mathbf{q}. \end{aligned}$$

The system can be described by its equation of motion

$$\mathbf{M}\ddot{\mathbf{q}} + \mathbf{K}\mathbf{q} = \hat{\mathbf{b}}\tau, \tag{4.1}$$

where $\mathbf{q}^\mathsf{T} = \begin{bmatrix}\theta & \mathbf{q}_e^\mathsf{T}\end{bmatrix}$, $\hat{\mathbf{b}} = \begin{bmatrix}1 & \mathbf{0}\end{bmatrix}^\mathsf{T}$,

$$\mathbf{K} = \begin{bmatrix} 0 & 0 \\ 0 & \mathbf{K}_{ee} \end{bmatrix},$$

and

$$\mathbf{M} = \begin{bmatrix} \mathbf{b}_3^\mathsf{T}\left(\mathbf{J} + \mathbf{J}_{tip}\right)\mathbf{b}_3 + I_{hub} & \mathbf{b}_3^\mathsf{T}\left(\mathbf{H} + \mathbf{H}_{tip}\right) \\ \left(\mathbf{H}^\mathsf{T} + \mathbf{H}_{tip}^\mathsf{T}\right)\mathbf{b}_3 & \mathbf{M}_{beam} + \mathbf{M}_{tip} \end{bmatrix}.$$

The contents of the mass and stiffness matrices are further described as

$$\mathbf{K}_{ee} = EI \int_0^L \mathbf{\Psi}''^\mathsf{T} \mathbf{\Psi}'' \mathrm{d}x,$$

where $\mathbf{\Psi}''$ is the second partial derivative of $\mathbf{\Psi}$ with respect to x, and

$$\mathbf{J} = \sigma \int_0^L \boldsymbol{\rho}_b^{\times\mathsf{T}} \boldsymbol{\rho}_b^{\times} \mathrm{d}x$$

is the second moment of inertia of the flexible appendage about the centre of the hub,

$$\mathbf{H} = \sigma \int_0^L \boldsymbol{\rho}_b^{\times} \mathbf{\Psi} \mathrm{d}x$$

is the matrix of modal angular momentum coefficients, and

$$\mathbf{M}_{beam} = \sigma \int_0^L \mathbf{\Psi}^\mathsf{T} \mathbf{\Psi} \mathrm{d}x.$$

Additionally,

$$\mathbf{J}_{tip} = m_{tip} \left(\boldsymbol{\rho}_b^{\times\mathsf{T}} \boldsymbol{\rho}_b^{\times}\right)_{x=L}$$

is the second moment of inertia of the tip mass about the centre of the hub,

$$\mathbf{H}_{tip} = m_{tip}\left(\boldsymbol{\rho}_b^{\times}\boldsymbol{\Psi}\right)_{x=L}$$

is the matrix of modal angular momentum coefficients of the tip, and

$$\mathbf{M}_{tip} = m_{tip}\left(\boldsymbol{\Psi}^{\mathsf{T}}\boldsymbol{\Psi}\right)_{x=L}.$$

4.1.2 Passivity Analysis

In this example, a passive mapping exists from a modified torque $\hat{\tau}_c = J_\theta^{-1}\tau$ to the μ-tip velocity $\dot{\rho}_\mu$. This is shown in the following analysis.

Assuming the tip mass is massive relative to the link's mass, the kinetic energy of the system can be decoupled as $T \approx T_\rho + T_e$, where T_ρ is the kinetic energy of the rigid hub and tip mass and T_e is the kinetic energy of the flexible appendage, given by

$$\begin{aligned} T_\rho &= \frac{1}{2}M_{\rho\rho}\theta^2 \\ T_e &= \frac{1}{2}\mathbf{q}_e^{\mathsf{T}}\mathbf{M}_{ee}\mathbf{q}_e, \end{aligned}$$

where

$$M_{\rho\rho} = \mathbf{b}_3^{\mathsf{T}}\left(\mathbf{J} + \mathbf{J}_{tip}\right)\mathbf{b}_3 + I_{hub},$$

and

$$\mathbf{M}_{ee} = \mathbf{M}_{beam} + \mathbf{M}_{tip}.$$

This approximation is based on the fact that the kinetic energy of the system is dominated by the kinetic energy of the rigid hub and tip mass when the tip is moving, and by the elastic kinetic energy when the tip is still [14].

The Hamiltonian of the decoupled system is

$$H = T_\rho + T_e + V,$$

and the Lagrangian of the decoupled system is

$$L = T_\rho + T_e - V.$$

By the principle of Virtual Work,

$$\begin{aligned}
\dot{\rho} &= J_\theta \dot{\theta} + \mathbf{J}_e \dot{\mathbf{q}}_e \\
\delta\rho &= J_\theta \delta\theta + \mathbf{J}_e \delta\mathbf{q}_e \\
\delta\theta &= J_\theta^{-1} \delta\rho - J_\theta^{-1} \mathbf{J}_e \delta\mathbf{q}_e,
\end{aligned}$$

where $J_\theta = r + l$ is the rigid Jacobian and $\mathbf{J}_e = \mathbf{\Psi}(l)$ is the elastic Jacobian. It can also be shown that

$$\begin{aligned}
\delta W &= \delta\theta\tau \\
&= \left(J_\theta^{-1} \delta\rho - J_\theta^{-1} \mathbf{J}_e \delta\mathbf{q}_e\right) \tau \\
&= \delta\rho \left(J_\theta^{-1} \tau\right) - \delta\mathbf{q}_e \left(J_\theta^{-1} \mathbf{J}_e \tau\right).
\end{aligned}$$

Therefore, from the approximately decoupled system,

$$\mathbf{M}_{\rho\rho}\ddot{\rho} = J_\theta^{-1}\tau \tag{4.2}$$

$$\mathbf{M}_{ee}\ddot{\mathbf{q}}_e + \mathbf{K}_{ee}\mathbf{q}_e = -J_\theta^{-1}\mathbf{J}_e\tau. \tag{4.3}$$

Next, consider the tip velocity, $\dot{\rho}$, where

$$\begin{aligned}\dot{\rho} &= (r+l)\,\dot{\theta} + \dot{\mathbf{u}}_e \\ &= J_\theta\dot{\theta} + \mathbf{J}_e\dot{\mathbf{q}}_e \\ &= \begin{bmatrix} J_\theta & \mathbf{J}_e \end{bmatrix}\dot{\mathbf{q}}.\end{aligned}$$

The μ-tip velocity of the tip mass,

$$\dot{\rho}_\mu = \begin{bmatrix} J_\theta & \mu\mathbf{J}_e \end{bmatrix}\dot{\mathbf{q}},$$

is an approximation of the real tip velocity, where $0 \leq \mu < 1$ [14]. When $\mu = 0$, the μ-tip velocity is the rigid tip velocity, and as μ approaches 1, the μ-tip velocity approaches the real tip velocity. Next, consider the nonnegative function [14]

$$\begin{aligned}H_\mu &= H - \mu(T_e + V_e) \\ &= T_\rho + T_e + V - \mu\,(T_e + V_e) \\ &= T_\rho + (1-\mu)\,(T_e + V_e)\,, \quad 0 \leq \mu < 1.\end{aligned}$$

Taking the time derivative of H_μ and using (4.1)−(4.3) gives

$$
\begin{aligned}
\dot{H}_\mu &= \dot{H} - \mu(\dot{T}_e + \dot{V}) \\
&= \dot{\mathbf{q}}^\mathsf{T}\mathbf{M}\ddot{\mathbf{q}} + \dot{\mathbf{q}}^\mathsf{T}\mathbf{K}\mathbf{q} - \mu\left(\dot{\mathbf{q}}_e^\mathsf{T}\mathbf{M}_{ee}\ddot{\mathbf{q}}_e + \dot{\mathbf{q}}_e^\mathsf{T}\mathbf{K}_{ee}\mathbf{q}_e\right) \\
&= \dot{\mathbf{q}}^\mathsf{T}\left(\mathbf{M}\ddot{\mathbf{q}} + \mathbf{K}\mathbf{q}\right) - \mu\left(\dot{\mathbf{q}}_e^\mathsf{T}\left(\mathbf{M}_{ee}\ddot{\mathbf{q}}_e + \mathbf{K}_{ee}\mathbf{q}_e\right)\right) \\
&= \dot{\mathbf{q}}^\mathsf{T}\left(\hat{\mathbf{b}}\tau\right) - \mu\dot{\mathbf{q}}_e^\mathsf{T}\left(-J_\theta^{-1}\mathbf{J}_e\tau\right) \\
&= \dot{\theta}\tau + \mu\dot{\mathbf{q}}_e^\mathsf{T}\left(J_\theta^{-1}\mathbf{J}_e\tau\right) \\
&= J_\theta J_\theta^{-1}\dot{\theta}\tau + \mu\dot{\mathbf{q}}_e^\mathsf{T}\left(J_\theta^{-1}\mathbf{J}_e\tau\right) \\
&= \left(J_\theta\dot{\theta} + \mu\dot{\mathbf{q}}_e^\mathsf{T}\mathbf{J}_e\right)J_\theta^{-1}\tau \\
&= \dot{\rho}_\mu\hat{\tau}_c.
\end{aligned} \tag{4.4}
$$

Integrating (4.4) gives

$$
\begin{aligned}
\int_0^T \dot{\rho}_\mu\hat{\tau}_c \mathrm{d}t &= H(T) - H(0) \\
&\geq -H(0),
\end{aligned}
$$

which proves that the map $\hat{\tau}_c \mapsto \dot{\rho}_\mu$ is passive.

4.1.3 Numerical Example

In this numerical example, the μ-tip rate is set to track the reference command

$$r(t) = 0.2\sin(\pi t).$$

This reference is a basic sinusoidal reference command. As a result, only one controller is necessary, and there is no gain-scheduling of controllers. When selecting an appropriate value of μ, a tradeoff must be made between performance and robustness. A low value of μ will lead to a more robust controller, while a larger value of μ will better represent the true payload velocity. For the purpose of this example, we will choose $\mu = 0.5$.

The tuning weights used to the design the LQG controller for the controller in Step 1 are $\mathbf{Q} = \mathrm{diag}\{1, 1\}$, $\mathbf{R} = 1$, $\mathbf{V} = \mathrm{diag}\{1, 1\}$, and $\mathbf{W} = 1$. The KYP lemma in Step 3 of the controller synthesis method is solved using `YALMIP` [15] and `MOSEK` [16] within `MATLAB`. The response of $\dot{\rho}_\mu$ and the tracking error in $\dot{\rho}_\mu$ are plotted in Figs. 4.2 and 4.3.

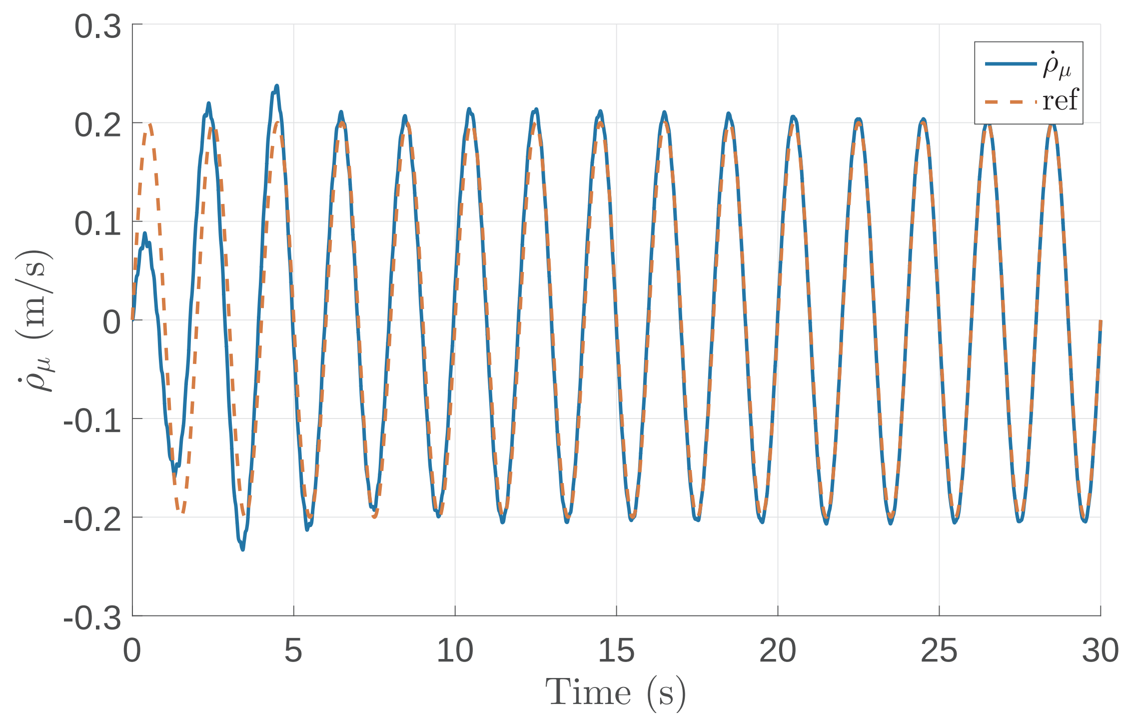

Fig. 4.2: Desired and actual μ-tip rate versus time.

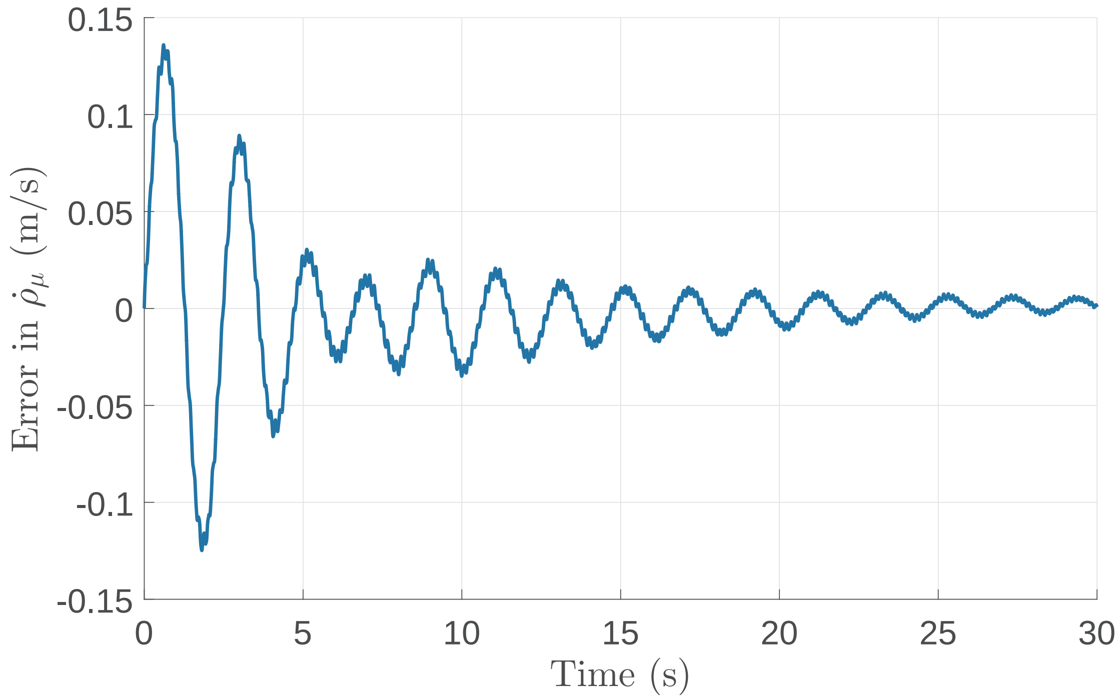

Fig. 4.3: μ-tip rate error versus time.

4.1.4 Discussion of Results

From Figs. 4.2 and 4.3, it is clear that the output tracks the reference command well and the tracking error quickly becomes very small. Fig. 4.4 displays the importance of Step 4 of the controller synthesis method proposed in Chapter 3, as the controller's phase changes from being unconstrained, to being constrained within $[-90, 90]$ degrees, confirming that the controller is PR.

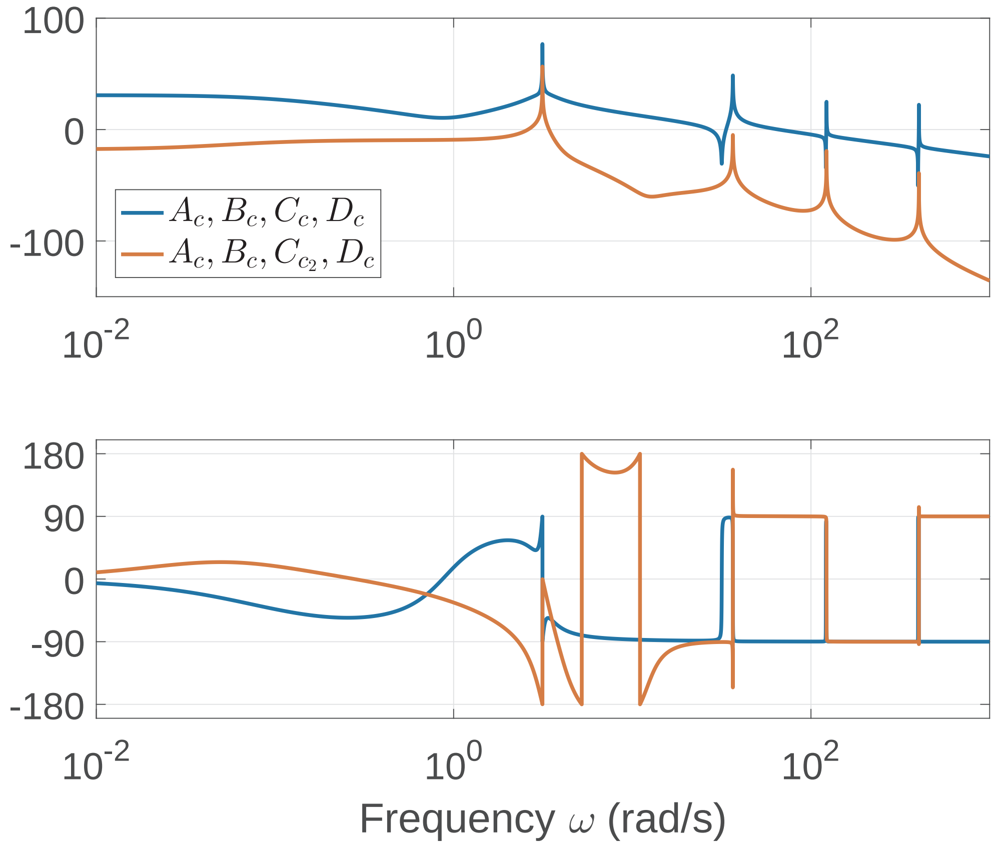

Fig. 4.4: Bode diagram of controller before (orange) and after (blue) Step 4 of the controller synthesis process.

4.2 Heat Exchanger

Consider a single tube-in-shell heat exchanger, shown in Fig. 4.5, involving hot and cold streams of benzine and aniline, respectively, with parameters from [17], listed in Table 4.2. Using the proposed controller synthesis method in Section 3, a gain-scheduled passive controller is designed to track a given reference command signal.

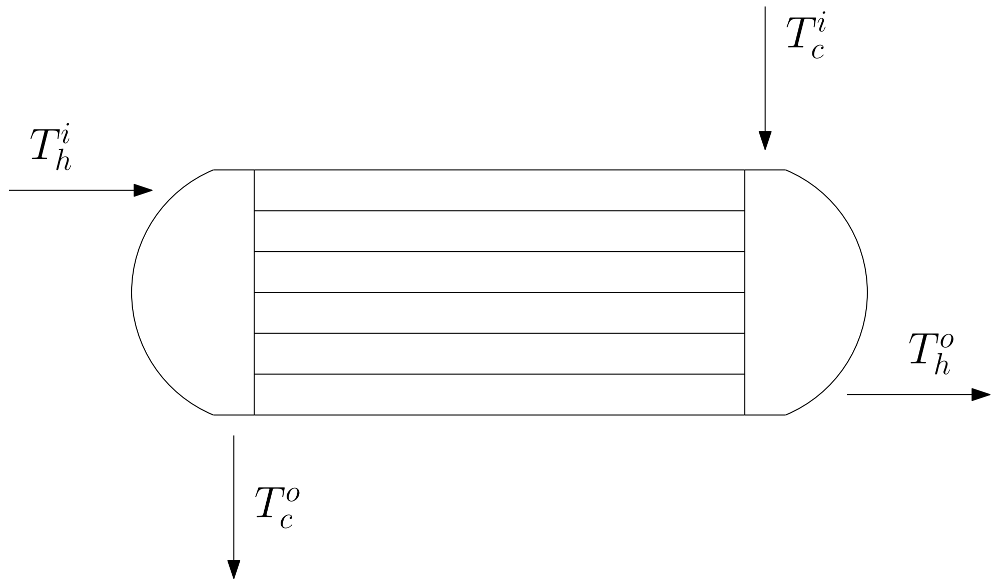

Fig. 4.5: Schematic of the single tube-in-shell heat exchanger used in the numerical example in Section 4.2.

4.2.1 System Modelling

A linear model approximating the dynamics of the heat exchanger temperature T_c^i is given in state-space form as [18]

$$\dot{\mathbf{T}}(t) = \mathbf{A}\mathbf{T}(t) + \mathbf{B}\mathbf{u}(t),$$

where

$$\mathbf{A} = \begin{bmatrix} -\frac{v_c}{V_c} - \frac{UA}{c_{pc}\rho_c V_c} & \frac{UA}{c_{pc}\rho_c V_c} \\ \frac{UA}{c_{ph}\rho_h V_h} & -\frac{v_h}{V_h} - \frac{UA}{c_{ph}\rho_h V_h} \end{bmatrix},$$

$$\mathbf{B} = \begin{bmatrix} \frac{v_c}{V_c} & 0 \\ 0 & \frac{v_h}{V_h} \end{bmatrix}, \quad \mathbf{T}(t) = \begin{bmatrix} T_c^o(t) \\ T_h^o(t) \end{bmatrix}, \quad \mathbf{u}(t) = \begin{bmatrix} T_c^i(t) \\ T_h^i(t) \end{bmatrix}.$$

The variable $T_j^k(t)$, $j = c, h$ and $k = i, o$, represents the temperature of the fluid, $\bar{T}_j^o$, $j = c, h$, represents the equilibrium outlet temperature of the fluid, v_j represents the volume flow rate, ρ_j is the fluid density, c_{pj} is the fluid specific heat, and V_j is the volume of each fluid. The variable U represents the heat transfer coefficient and A represents the area. Subscripts c and h indicate the cold or hot stream, while superscripts i and o indicate properties at the inlet or outlet of a stream. Flow rates and physico-chemical properties are assumed constant throughout the exchanger.

If the cold inlet temperature is chosen to be some fixed value, the model can be simplified to a SISO model, described by

$$\delta\dot{\mathbf{T}}(t) = \mathbf{A}_p \delta\mathbf{T}(t) + \mathbf{B}_p u(t),$$

where

$$\mathbf{A}_p = \mathbf{A} = \begin{bmatrix} -\frac{v_c}{V_c} - \frac{UA}{c_{pc}\rho_c V_c} & \frac{UA}{c_{pc}\rho_c V_c} \\ \frac{UA}{c_{ph}\rho_h V_h} & -\frac{v_h}{V_h} - \frac{UA}{c_{ph}\rho_h V_h} \end{bmatrix}, \quad \mathbf{B}_p = \begin{bmatrix} 0 \\ \frac{v_h}{V_h} \end{bmatrix},$$

$\delta\mathbf{T}(t) = \mathbf{T}(t) - \bar{\mathbf{T}} = \begin{bmatrix} T_c^o(t) & T_h^o(t) \end{bmatrix}^\mathsf{T} - \begin{bmatrix} \bar{T}_c^o & \bar{T}_h^o \end{bmatrix}^\mathsf{T}$,$u(t) = T_h^i(t)$, $\bar{T}_c^o$ is the equilibrium cold outlet temperature, and $\bar{T}_h^o$ is the equilibrium hot outlet temperature.. A measurement of $y = \mathbf{C}_p \delta\mathbf{T} = \begin{bmatrix} 1 & 0 \end{bmatrix} \delta\mathbf{T}(t) = T_c^o(t) - \bar{T}_c^o$ is assumed to be available.

4.2.2 Numerical Example

In this numerical example, the cold stream input is set to a constant temperature of $T_c^i = 30$°C, which leads to equilibrium output temperatures of $\bar{T}_c^o = 23.0$°C and $\bar{T}_h^o = 16.8$°C. In simulation, the initial conditions are set as $T_c^o(0) = 30$°C and $T_h^o(0) = 30$°C. A triangular wave with an offset is chosen as the reference command for the hot stream outlet, given by

$$T_{ref}(t) = a_0 + 4\frac{a}{p}\left(\left|(t \text{ modulo } p) - \frac{p}{2}\right| - \frac{p}{4}\right), \tag{4.5}$$

where a_0 is the offset, a is the amplitude of the triangle wave and p is its period. The numerical parameters used to describe the reference signal are listed in Table 4.3. Alternatively, the reference signal in (4.5) can be described by the Fourier series

$$T_{ref}(t) = a_0 + \sum_{k=0}^{\infty} a_k (-1)^k \frac{\sin(2\pi(2k+1)ft)}{(2k+1)^2},$$

where the frequency f is the inverse of the period p.

Table 4.2: Numerical parameters describing the heat exchanger in the numerical example.

Parameters	**Units**	**Benzene (Hot)**	**Aniline (Cold)**
U	$\frac{\text{J}}{\text{s}\cdot\text{m}^2\cdot{}^\circ\text{C}}$	391	–
A	m^2	7.57	–
v	$\frac{\text{m}^3}{\text{s}} \times 10^{-4}$	7.17	12.0
ρ	$\frac{\text{kg}}{\text{m}^3}$	879	1022
c_p	$\frac{\text{J}}{\text{kg}\cdot{}^\circ\text{C}} \times 10^3$	1.76	2.18
V	$\text{m}^3 \times 10^{-2}$	3.75	9.41

Table 4.3: Numerical parameters describing the reference signal used in the heat exchanger numerical example.

Parameters	**Variable**	**Value**	**Units**
Offset	a_0	40	°C
Amplitude	a	5	°C
Period	p	120	s
Frequency	f	$\frac{1}{120}$	s^{-1}

In order to track the reference signal, the controller is designed to contain internal models of the sinusoidal modes in the Fourier series that make up the reference signal. In particular, the controller must contain at least one pole at $s = 0$ to track the step input, as well as poles at $s = \pm(2n+1)2\pi fj$, $n \in \mathbb{N}$ to track each mode of the reference signal. In practice, only a

Table 4.4: Numerical parameters of the scheduling signal used in the numerical example.

Variable	**Value**	**Variable**	**Value**
a_0	1	$s_{0,0}$	0.0001
a_1	7	$s_{1,0}$	0.2
a_2	7/3	$s_{2,0}$	0.2/3
a_3	7/5	$s_{3,0}$	0.2/5
a_4	7/7	$s_{4,0}$	0.2/7
a_5	7/9	$s_{5,0}$	0.2/9
a_6	7/11	$s_{6,0}$	0.2/11
a_7	7/13	$s_{7,0}$	0.2/13
a_8	7/15	$s_{8,0}$	0.2/15
a_9	7/17	$s_{9,0}$	0.2/17

finite number of reference signal modes can be implemented, and in this particular example the controller includes an integrator and the first nine modes of the Fourier series. The tuning weights used to the design the LQG controller for each individual controller in Step 1 are $\mathbf{Q} = \text{diag}\{1, 1\}$, $\mathbf{R} = 1$, $\mathbf{V} = \text{diag}\{1, 1\}$, and $\mathbf{W} = 1$. The KYP lemma in Step 3 of the controller synthesis method is solved using `YALMIP` [15] and `MOSEK` [16] within `MATLAB`.

The scheduling signals of the controller in this numerical example are given by

$$s_j(t) = \begin{cases} \left(\frac{a_j - s_{j,0}}{\bar{t}}\right) t + s_{j,0} & t \leq \bar{t} \\ a_j & t > \bar{t} \end{cases}, \; j = 0, \ldots, 9,$$

where a_j, $j = 0, \ldots, 9$, are the Fourier coefficients of the reference signal; $s_{j,0}$, $j = 0, \ldots, 9$, are initial values of the scheduling signals at $t = 0$ min; and $\bar{t} = 10$ min is the time at which the scheduling signals switch from linear varying to constant. The numerical values of a_j and $s_{j,0}$, $j = 0, \ldots, 9$, are given in Table 4.4. The controllers are scheduled based on the Fourier coefficients to best represent the influence of each internal model in the reference signal being

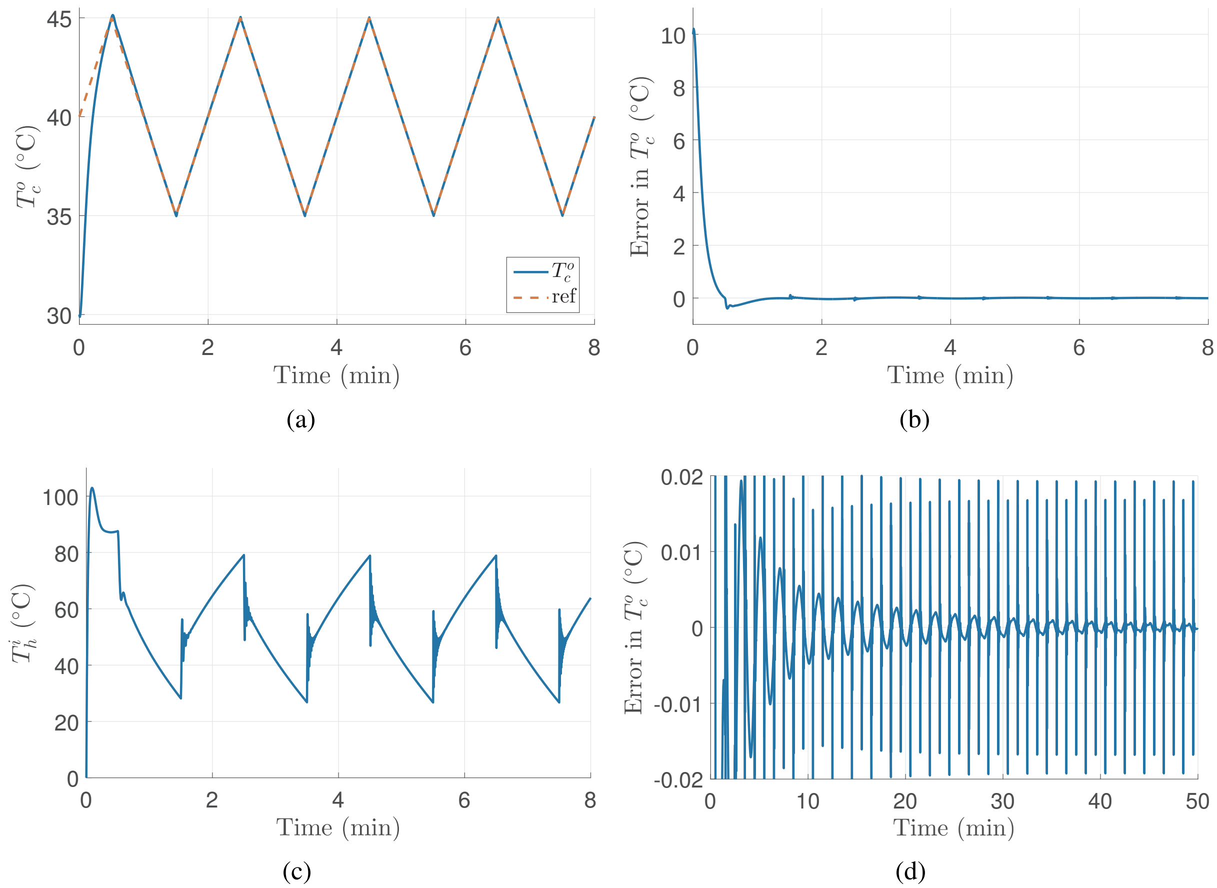

Fig. 4.6: Plots of (a) T_c^o and desired output versus time, (b) tracking error versus time, (c) control input T_h^i versus time, and (d) enlarged view of tracking error versus time for the numerical example of Section 4. The simulation is performed for 50 min, but only results from the first 8 min are presented in (a)-(c).

tracked.

Closed-loop simulation results with the controller designed to include internal models of the first nine Fourier series modes of the reference command are presented in Fig. 4.6.

4.2.3 Discussion of Results

From Figs. 4.6(a) and 4.6(b) it is apparent that the reference command signal is tracked well and the tracking error becomes small quickly. In the enlarged plot of Fig. 4.6(d), sharp spikes in the tracking error can be seen at the times where the reference command is non-smooth, but otherwise the steady-state tracking error is tending towards zero. The sharp spikes in tracking error are most likely due to the fact that only a finite number of Fourier series modes are being implemented as internal models. As the number of modes used is increased, it is expected that the magnitude of the spikes will decrease.

Chapter 5

Conclusion

5.1 Final Remarks

The controller design method presented in this thesis leads to a passive controller that includes a number of internal models. Inspired by the internal model principle, the internal models of the controller lead to a reduction in steady-state tracking error. The gain-scheduled nature of the controller makes it very simple to tune the internal models for a variety of reference commands. As done in the heat exchanger numerical example in Chapter 4, a Fourier series representation of the reference command signal can be obtained and the first N modes can be used as internal models. The scheduling signals of each individual controller can be chosen based on the Fourier coefficients.

5.2 Future Work

Future work on this topic will examine the effect that choosing different number of Fourier series modes has on the tracking performance and look into applying this controller synthesis to disturbance rejection problems.

Currently this controller has been tested on two simulated systems, a flexible-link manipulator and a single tube-in-shell heat exchanger. Eventually, this controller will be validated experimentally on test platforms, including various configurations of flexible-link manipulators.

References

[1] B. Brogliato, R. Lozano, B. Maschke, and O. Egeland, *Dissipative Systems Analysis and Control: Theory and Applications*, 2nd ed. Springer, 2007.

[2] B. Francis and W. Wonham, "The internal model principle of control theory," *Automatica*, vol. 12, no. 5, pp. 457–465, 1976.

[3] K. C. Cheok, N. K. Loh, and J. B. Ho, "Continuous-time optimal robust servo-controller design with internal model principle," *International Journal of Control*, vol. 48, no. 5, pp. 1993–2010, 1988.

[4] R. Ortega, *Passivity-based control of Euler-Lagrange systems*, 1st ed. Springer, 1998.

[5] C. J. Damaren, "Gain-scheduled SPR controllers for nonlinear flexible systems," *Journal of Dynamic Systems, Measurement, and Control*, vol. 118, no. 4, pp. 698–703, 1996.

[6] J. R. Forbes and C. J. Damaren, "Design of gain-scheduled strictly positive real controllers using numerical optimization for flexible robotic systems," *Journal of Dynamic Systems, Measurement, and Control*, vol. 132, no. 3, May 2010.

[7] P. C. Hughes, *Spacecraft Attitude Dynamics*, 2nd ed. Dover, 2004.

[8] A. H. de Ruiter, C. Damaren, and J. R. Forbes, *Spacecraft Dynamics and Control: An Introduction*, 1st ed. Wiley, 2013.

[9] C. A. Desoer and M. Vidyasagar, *Feedback Systems: Input-Output Properties*. New York, NY: Academic Press., 1975, ch. 4.

[10] H. J. Marquez, *Nonlinear Control Systems: Analysis and Design*. Hoboken, NJ: John Wiley, 2003.

[11] H. Sane and D. Bernstein, "Asymptotic disturbance rejection for Hammerstein positive real systems," *IEEE Transactions on Control Systems Technology*, vol. 11, no. 3, pp. 364–374, 2003.

[12] J. R. Forbes, *Extensions of Input-Output Stability Theory and the Control of Aerospace Systems*. Ph.D. Thesis, University of Toronto, 2011.

[13] J. W. Nilsson and S. A. Riedel, *Electric circuits*. Prentice Hall, 2000.

[14] C. Damaren, "Approximate inverse dynamics and passive feedback for flexible manipulators with large payloads," *IEEE Transactions on Robotics and Automation*, vol. 12, no. 1, pp. 131–138, 1996.

[15] J. Löfberg, "`YALMIP`: A toolbox for modeling and optimization in `MATLAB`," in *Proceedings of the CACSD Conference*, Taipei, Taiwan, 2004.

[16] M. ApS, *The MOSEK optimization toolbox for MATLAB manual. Version 7.1 (Revision 28).*, 2015. [Online]. Available: http://docs.mosek.com/7.1/toolbox/index.html

[17] R. W. Serth, *Process heat transfer*. Academic Press/Elsevier, 2007.

[18] J. Bao and P. L. Lee, *Process Control: The Passive Systems Approach*. London, UK: Springer, 2007.